

The Recent Increase in the Occurrence of a Boreal Summer Teleconnection and Its Relationship with Temperature Extremes

MIN-HEE LEE

Korea Polar Research Institute, Incheon, and School of Earth and Environmental Sciences, Seoul National University, Seoul, South Korea

SUKYOUNG LEE

School of Earth and Environmental Sciences, Seoul National University, Seoul, South Korea, and Department of Meteorology, The Pennsylvania State University, University Park, Pennsylvania

HYO-JONG SONG

Korea Institute of Atmospheric Prediction Systems, Seoul, South Korea

CHANG-HOI HO

School of Earth and Environmental Sciences, Seoul National University, Seoul, South Korea

(Manuscript received 25 January 2016, in final form 8 June 2017)

ABSTRACT

This study has investigated the relationship between temperature extremes and a subseasonal hemispheric teleconnection pattern over the Northern Hemisphere during boreal summer. By applying self-organizing map (SOM) analysis to 200-hPa geopotential fields from the European Centre for Medium-Range Weather Forecasts interim reanalysis (ERA-Interim) for the period 1979–2012, a teleconnection pattern is identified that increased dramatically in its occurrence after the late 1990s. This pattern is characterized by a zonal wavenumber-5 pattern with anomalous high pressure cores over eastern Europe, northeastern Asia, the eastern North Pacific, the eastern United States, and Greenland. These high pressure centers coincide with regions of increasingly frequent temperature extremes in recent decades. To investigate the temporal evolution of the identified SOM pattern, time-lagged composites were performed relative to the days in which the 200-hPa geopotential field most closely resembled the SOM pattern. From day -10 to day 0, a wave train propagated from the central tropical Pacific to the Canadian Arctic Archipelago and Greenland. This poleward wave propagation was followed by the establishment of quasi-stationary high pressure centers over Greenland, Europe, and Asia. This study suggests that more frequent occurrence of the hemispheric teleconnection is linked to more severe and longer extreme weather events over the Northern Hemisphere since the late 1990s.

1. Introduction

In recent decades, an upward trend has been reported in the occurrence of extreme weather events around the world (e.g., Alexander et al. 2006; Peterson and Manton 2008; Hansen et al. 2010; Rahmstorf and Coumou 2011; IPCC 2012; Seneviratne et al. 2014). During the summer of 2010, many regions including the eastern United States, Middle East, eastern Europe, Russia, and northeastern China experienced record-breaking high

temperatures, and many regions over Pakistan, the southern United States, and Australia experienced extremely heavy rainfall and flooding (Barriopedro et al. 2011; Huber and Gullede 2011; Lau and Kim 2012; Schneiderei et al. 2012). Such weather events and climate extremes have become a growing concern because they often cause disasters that affect human lives, the economy, and the ecosystem (Trenberth et al. 2007; Lee et al. 2012). It has been suggested that positive trends in certain extremes are caused by global warming (e.g., Alexander et al. 2006; Rahmstorf and Coumou 2011; IPCC 2012), although it is difficult to rule out the effects

Corresponding author: Min-Hee Lee, mhlee@kopri.re.kr

DOI: 10.1175/JCLI-D-16-0094.1

© 2017 American Meteorological Society. For information regarding reuse of this content and general copyright information, consult the [AMS Copyright Policy](http://www.ametsoc.org/PUBSReuseLicenses) (www.ametsoc.org/PUBSReuseLicenses).

of natural variability such as El Niño–Southern Oscillation (ENSO) (Lau 1997; Arblaster and Alexander 2010; Cai et al. 2014, 2015).

Regardless of the root cause, for the case of persistent extremes such as heat waves and drought, large-scale atmospheric circulations apparently play an important role. For example, atmospheric blocks can induce heat waves, droughts, and flooding by prohibiting the downstream propagation of ridges and troughs (Dole et al. 2011; Hong et al. 2011; Lau and Kim 2012). Hemispheric teleconnection patterns, including circumglobal teleconnection (CGT) (Branstator 2002, Ding and Wang 2005) and Silk Road patterns (Enomoto et al. 2003; Wang et al. 2012), may also be linked to extremes because of their slow phase speeds. Indeed, Teng et al. (2013) used this quasi-stationary property of the CGT pattern to predict U.S. heat waves.

Given the increase in the occurrence of extreme events that are connected to large-scale atmospheric circulation, it is important to determine whether attendant changes are present in certain large-scale circulation pattern during the boreal summer [June–August (JJA)]. It has been shown that a cluster analysis, known as the self-organizing map (SOM) method, can be used to identify and to distinguish atmospheric jet shift patterns that are too similar to be separated by empirical orthogonal functions (EOFs) but are nevertheless associated with distinct forcing mechanisms (Lee and Feldstein 2013; Feldstein and Lee 2014). Using the same method, Johnson (2013) identified a continuum of ENSO sea surface temperature (SST) patterns. These results stem from the fact that SOM patterns can more accurately represent actual observed events than EOFs (Liu et al. 2006; Johnson et al. 2008).

Consistent with these findings, Bao and Wallace (2015) analyzed 500-hPa height fields and concluded that clusters derived from SOMs are more linearly independent than clusters derived from commonly used hierarchical cluster analysis, and that SOM clusters are more distinctive from each other in terms of the Euclidean distances between the centroids. Bao and Wallace (2015) identified four SOM patterns that are robust and showed that these patterns represent circulations that are important for boreal winter climate in North America and Europe. Moreover, they found that these SOM patterns are useful for interpreting flow patterns that occurred during the abnormal winters of 1930/31, 2009/10, and 2013/14. Because we are interested in extremes, this finding provides an additional impetus for adopting the SOM method as our analysis method.

In section 2, we provide a detailed description of the analysis method. As shown in section 3, this analysis reveals a sudden increase in the occurrence of a

CGT-like pattern in the late 1990s. Moreover, this large-scale pattern is associated with extreme temperatures over Europe, East Asia, and the east-central United States. A possible forcing mechanism of this CGT-like pattern is explored in section 4, and a summary and discussion are presented in section 5.

2. Data and methods

a. Data

This study analyzed the daily fields of the European Centre for Medium-Range Weather Forecasts (ECMWF) interim reanalysis (ERA-Interim) dataset (Dee et al. 2011) for the boreal summers of 1979–2012. The analyzed variables include 200-hPa geopotential (Z200), zonal wind, meridional wind, 2-m temperature, and daily maximum temperature. The choice of Z200 is based on previous studies on summer teleconnection patterns (e.g., Ding and Wang 2005; Lee et al. 2011; Ha et al. 2012; Saeed et al. 2014). The SOM analysis is performed on deseasonalized Z200 fields. For the lag-composite analysis, however, each JJA mean is also removed.

b. Extreme indices

Among various extreme indices, we adopted two extreme temperature indices from the Expert Team on Climate Change Detection and Indices (ETCCDI) that have been widely used to detect changes in extremes (Alexander et al. 2006; Peterson and Manton 2008). The first index is the annual (in this study, JJA only) maximum of daily maximum temperature (maxTX). This index measures the amplitude of extreme events. The second index is the warm spell duration index (WSDI), defined as the number of periods in which at least six consecutive days had daily maximum temperature greater than the 90th percentile value of historical records. The WSDI measures the persistence of hot extremes.

c. Self-organizing map

SOM analysis is a cluster method based on neural networks. Similar to *K*-means clustering, it classifies data into a specified number of clusters. Compared with hierarchical clustering (e.g., Ward's method; Ward 1963), which develops clusters by merging clusters of the previous step, SOM analysis uses all data simultaneously during the training period. After the pattern learning, SOM analysis orders cluster patterns by placing them in a one- or two-dimensional grid such that neighboring SOM patterns have geometrical similarity (Kohonen 2001). For this reason, previous studies have used this

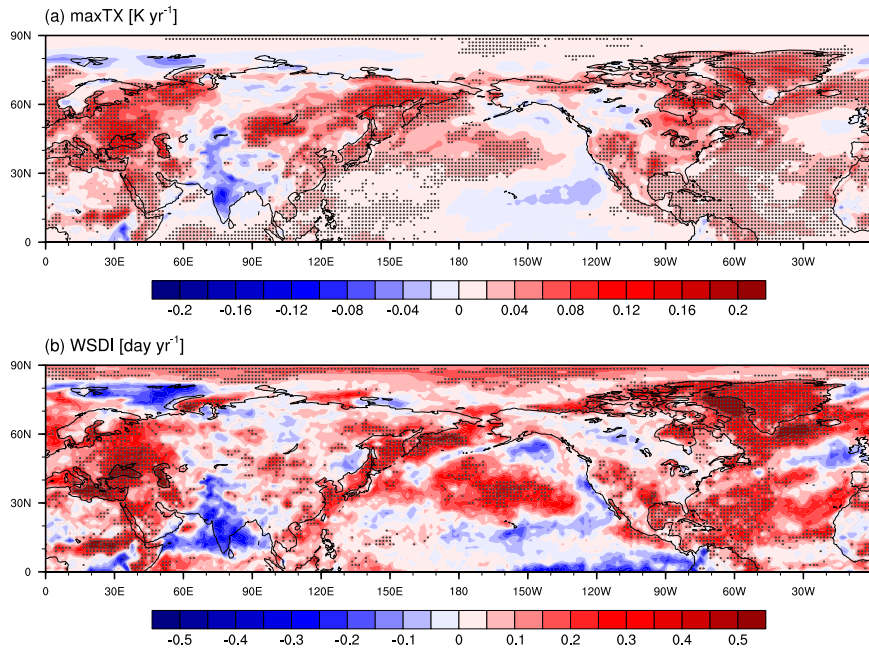


FIG. 1. Trends of (a) maxTX and (b) WSDI for 1979–2012. The dots denote regions in which the trends exceed the 95% confidence level, as determined by the two-sided Student's t test.

analysis to describe a continuum in atmospheric teleconnection patterns (e.g., [Leloup et al. 2007](#); [Johnson et al. 2008](#); [Johnson 2013](#)). [Yuan et al. \(2015\)](#) showed for boreal winter that their SOM patterns more closely resemble observed daily data than their EOF counterparts do. For more detailed information on the application of SOM analysis, we refer the reader to the appendix in [Johnson et al. \(2008\)](#).

SOM patterns are determined by a minimization of the Euclidean distance between the SOM patterns (the centroids) and the data. In our case, the data are the daily Z200 fields. For each daily Z200 field, one can identify a best matching SOM pattern by defining it as the SOM pattern that has the smallest Euclidean distance between itself and the daily field. The match (reduction in Euclidean distance) improves as the number of SOM patterns increases. Therefore, it is preferable that 1) the number of SOM patterns is large enough to accurately capture the patterns of the daily data and, in order for the cluster patterns to be useful, that 2) the number of SOM patterns should be sufficiently small that the clusters are distinctive from each other. To determine the number of SOM patterns that satisfies both of these two criteria, we follow [Lee and Feldstein \(2013\)](#) and compute average pattern correlations between the daily fields and their best matching SOM pattern. We also compute the distance between different cluster pairs d using the following definition:

$$d(r, s) = \sqrt{\frac{2n_r n_s}{(n_r + n_s)} \|\bar{x}_r - \bar{x}_s\|_2}, \quad (1)$$

where n_r and n_s are the number of elements in clusters r and s , respectively, and \bar{x}_r and \bar{x}_s are the centroid patterns of clusters r and s , respectively. This equation was adopted from Ward's concept of merging cost that can be considered as the cost of combining two clusters. Although SOM is not a hierarchical cluster method, the merging cost can be used to measure the distinctiveness of any two clusters ([Xu et al. 2013](#)). As will be described subsequently, a (5×1) (i.e., 5 rows by 1 column) SOM grid satisfies the two criteria: relatively high pattern correlations and relatively large inter-SOM distances.

3. Temperature extremes and teleconnections

[Figure 1](#) displays the trends in temperature extremes during the 1979–2012 study period. Many regions over the Northern Hemisphere, particularly eastern Europe, central Asia, northeastern Asia, Russia, the central United States, and Greenland, have experienced frequent extreme high temperatures in recent years; these results are consistent with previous research ([Seneviratne et al. 2014](#)). A comparison of [Figs. 1a and 1b](#) reveals that in terms of extreme persistence, as quantified by the WSDI, the area of statistically significant trends is more limited than that of the temperature

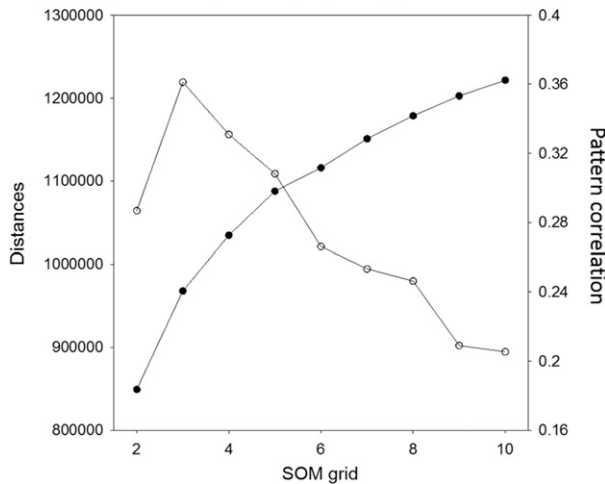


FIG. 2. Mean pattern correlation among the geopotential at 200 hPa field, the best-matching SOM pattern (closed circle, right y axis), and the Euclidean distances (gpm) between SOM patterns (open circle, left y axis) as a function of a single-column SOM grid.

itself. However, over eastern Europe, the central United States, and Greenland, the WSDI trend is significantly positive. These core regions appear to form a wave pattern, suggesting that the extreme changes may be associated with hemispheric-scale Rossby wave teleconnections.

To explore this possibility, we applied SOM analysis to Z200 over the Northern Hemisphere extratropics. The horizontal domain is confined to the latitudes between 20° and 90°N. To determine an appropriate number of SOM clusters that is large enough to produce clusters that accurately describe the daily fields, we varied the grid from (2 × 1) to (10 × 1), and for each grid we calculated the mean pattern correlation between the best matching SOM pattern and the daily fields. The result is indicated by the closed circles in Fig. 2. Next, to determine the grid for which the resulting SOM patterns are distinct from each other, the average Euclidean distances between all possible pairs of SOM patterns were calculated, and then averaged. For example, for a (2 × 1) grid, there is only one pair; for a (3 × 1) grid, there are two pairs. The result is shown by the open circles in Fig. 2. From these results, we chose a (5 × 1) grid because the pattern correlation, 0.31, was statistically significant at the 95% confidence level, while the average distance between SOM patterns decreased only incrementally as the number of grids increased from (2 × 1) to (5 × 1), and decreased markedly as the SOM grid size increased from (5 × 1) to (6 × 1). The statistical significance test was performed with a Monte Carlo method; we generated bootstrapped samples of mean pattern correlations from 1000 random samples. Each sample correlation was calculated with N randomly

selected daily anomalies, where N is the number of matching days for a particular SOM pattern ($N = 582, 623, 634, 671,$ and 618 for the first to fifth SOM, respectively).

The resulting spatial patterns and their annual (JJA) frequency of occurrence are shown in Fig. 3. Here, for each SOM pattern, the frequency of occurrence was measured by counting the number of days showing the best match with a particular SOM pattern (i.e., the smallest Euclidean distance between the observed daily pattern and the SOM pattern). Consistent with previous studies of atmospheric teleconnections, the time scales of the SOMs are short, with e -folding time scales being 4.7, 4.5, 4.2, 4.4, and 4.8 days for the first to fifth SOM, respectively. For each SOM, the e -folding time was computed using a projection time series $P(t)$, which was obtained by projecting daily 200-hPa geopotential anomalies Φ' onto the SOM pattern Φ^* (Johnson and Feldstein 2010; Goss et al. 2016):

$$P(t) = \frac{\sum_i \sum_j \Phi'(\lambda_i, \theta_j, t) \Phi^*(\lambda_i, \theta_j) \cos \theta_j}{\sum_i \sum_j [\Phi^*(\lambda_i, \theta_j)]^2 \cos \theta_j}, \quad (2)$$

where λ_i is the longitude at zonal grid point i , θ_j is the latitude at meridional grid point j , and t is time. Teleconnection patterns with similarly short e -folding time scales often have substantial variability at interannual and longer time scales. While intrinsic long-term variability such as ENSO can help account for the longer time-scale variability, much of this variability arises from climate noise (Leith 1973; Madden 1976; Feldstein 2000).

By construction, the SOM patterns positioned in the neighboring SOM grid locations are similar to each other with relatively small Euclidean distance between them, and those at distant SOM grid locations are increasingly different from each other. Therefore, the first and the fifth SOMs are almost out of phase with each other. The first SOM (SOM1; Fig. 3a) resembles the negative phase of the CGT pattern, which is associated with cooling events over negative-anomaly regions in 2009 such as the North Atlantic, central Asia, East Asia, the North Pacific, and the northeastern United States [Fig. 1 in Ha et al. (2012)]. It is also worthwhile to mention that the frequency of occurrence of SOM1 had been decreasing with the exception of 2009. Since the SOM1 pattern is approximately opposite to the fifth SOM (SOM5) pattern, this negative trend in SOM1 is consistent with the positive trend in SOM5. Again, this decline in SOM1 frequency could also be caused by the additive effect of the Z200 trend. For the second pattern (SOM2; Fig. 3b), the Atlantic sector deviated from

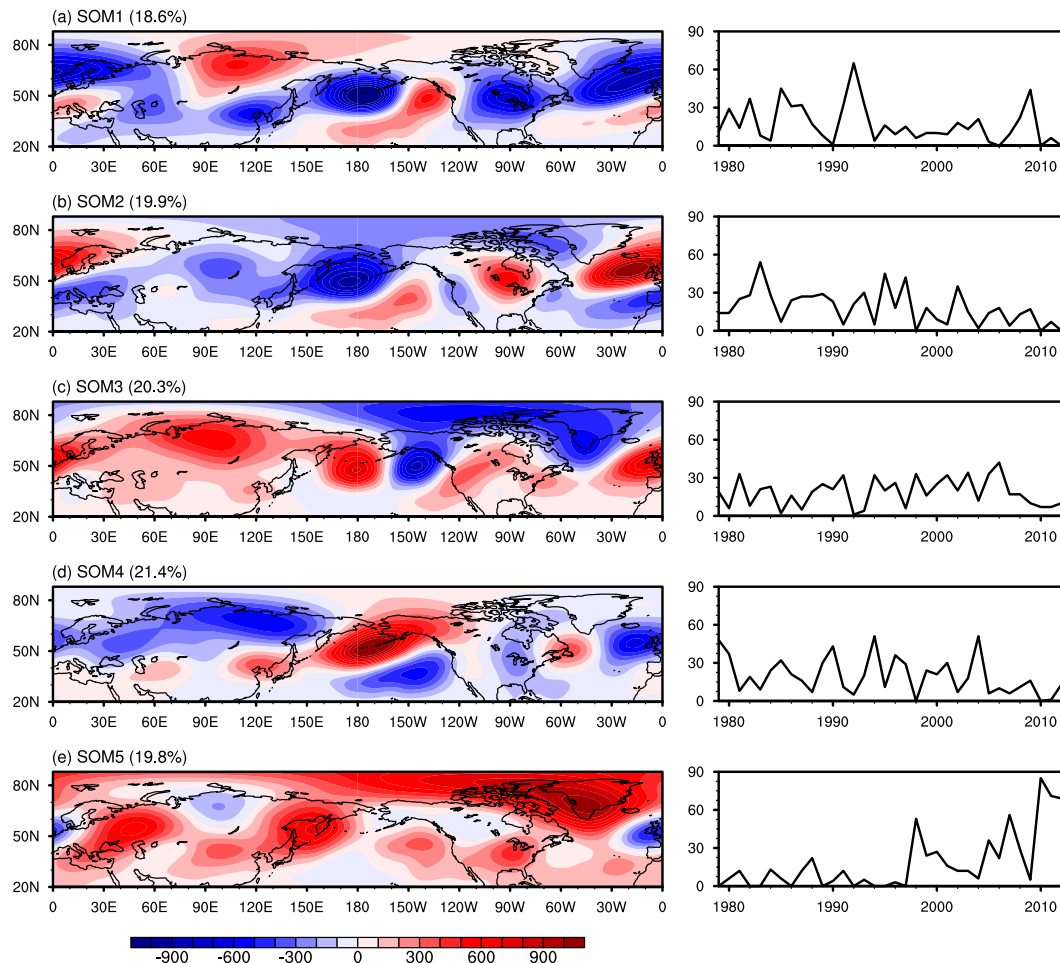


FIG. 3. (left) Geopotential at 200 hPa ($\text{m}^2 \text{s}^{-2}$) SOM patterns and (right) their annual frequency of occurrence indicated by the number of days per each JJA season. The percentage for each set indicates the frequency of occurrence of the corresponding pattern for 1979–2012 boreal summers.

SOM1, whereas the circulation over the Eurasian continent showed a close resemblance to SOM1. The third pattern (SOM3; Fig. 3c), can be overall characterized by negative anomalies over the polar region and positive anomalies over midlatitudes. The fourth pattern (SOM4; Fig. 3d) was overall similar to SOM2 in structure but had an opposite sign. No notable changes were noted in the frequency of occurrence in SOM1–SOM4 during 1979–2012.

The last pattern, SOM5, showed a dramatic increase in occurrence during the late 1990s (Fig. 3e). It is worth noting that in 2010, when many regions over the Northern Hemisphere experienced various extremes (Barriopedro et al. 2011; Huber and Gullede 2011; Lau and Kim 2012; Schneidereit et al. 2012), most JJA days, 85 of the total 92 days, were classified as SOM5. The spatial pattern is characterized by positive anomalies over most regions with the exception of an isolated

region centered over the United Kingdom and northern Siberia. It is interesting to note that the positive centers over Greenland, eastern Europe, northeastern Asia, and the east-central United States coincided with regions in which the extremes increased as revealed by a comparison of Figs. 3e and 1. Even though SOM5 represents a Z200 anomaly and not a surface anomaly, the pattern correlation between SOM5 (Fig. 3e) and maxTX (Fig. 1a) is 0.63, significant at the 95% confidence level. There are some exceptions to this correspondence: the high over the Gulf of Alaska with no corresponding extremes, and the increased extremes over North Pacific and the Gulf of Mexico with no large-scale high anomalies. Because these exceptions occur over the ocean, we speculate that the lack of correspondence may be in part caused by the presence of large natural variability, such as ENSO or the Pacific decadal oscillation, which influences SST.

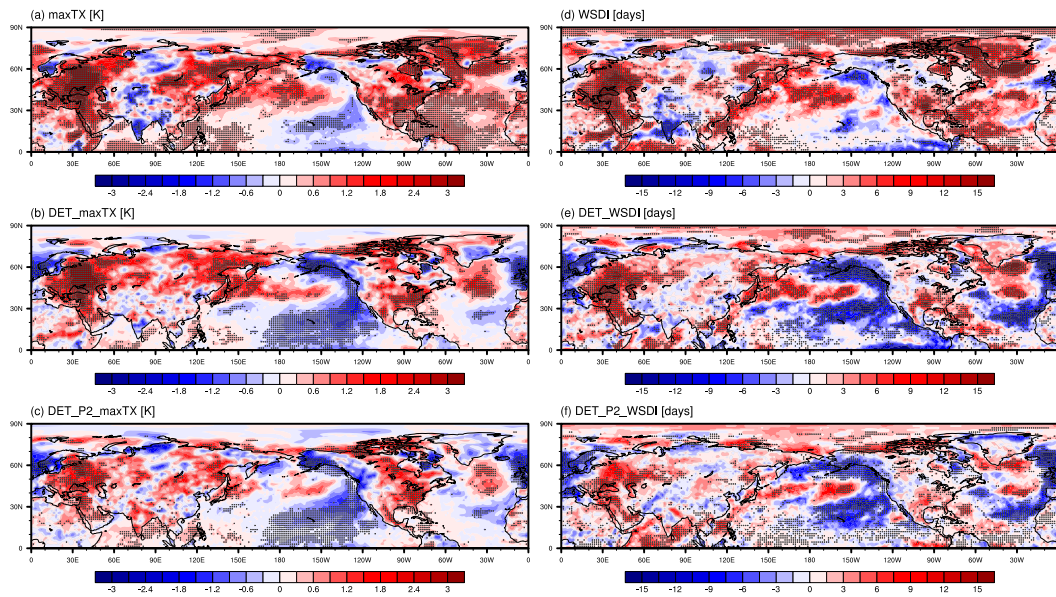


FIG. 4. Composite difference among the highest and lowest five years in the SOM5 frequencies for (a) maxTX, (b) the detrended maxTX, (c) the detrended maxTX for P2, (d) WSDI, (e) the detrended WSDI, and (f) the detrended WSDI for P2. The dots denote regions in which the differences exceeded the 95% confidence level by the Monte Carlo method.

As an additional test, we computed how many extremes occur on those days when the circulation matches SOM5. Compared with the earlier period when SOM5 occurred rarely, we found that during the period of 1998–2012, over the SOM5's high pressure core regions, about 70% of the extreme event days occur during the days that match SOM5 (not shown). Therefore, while there are other factors that influence summer temperature extremes, our calculation indicates that the atmospheric circulation pattern represented by SOM5 is linked to the majority of the extreme events. The tight relationship between the circulation and the extreme temperature is underscored by the high correlation coefficient, 0.74, between maxTX (Fig. 4) and the changes in 2-m temperature (T2m) associated with SOM5 (not shown). It is noteworthy that certain aspects of the SOM5 pattern—a zonal wavenumber-5 pattern and high pressure centers over eastern Asia and eastern North America—also resemble the CGT pattern (Branstator 2002), which has been shown to be linked to temperature and precipitation anomalies (Ding and Wang 2005).

4. Trend and interannual variability of extremes associated with SOM5 occurrence

The findings presented in section 3 suggest that the teleconnection described by SOM5 is closely tied to the recent upward trend in boreal summer temperature extremes (Fig. 1; Alexander et al. 2006; Peterson and

Manton 2008; Hansen et al. 2010; Rahmstorf and Coumou 2011; IPCC 2012; Seneviratne et al. 2014). To explore this possibility, we analyzed the composite differences in maxTX and WSDI based on the occurrence of SOM5 during the top five years (2010, 2011, 2012, 2008, and 1998) and the bottom five years (1979, 1982, 1983, 1986, and 1989). The sample number of five years was chosen because it corresponds to the top and bottom 15th percentile of the SOM5 occurrence for each JJA during the 34 years of 1979–2012. We have found that the composites with the top and bottom four, six, and seven years are insensitive to the number of years used for the composite (not shown). The significance of the composite was evaluated by using a Monte Carlo test in which two sets of 5 years from the total 34 years were randomly drawn, and the composites of extremes for these two sets and their differences were calculated. This procedure was repeated 1000 times, and the resulting values were used to determine the 95% confidence levels.

During the years in which the flow pattern closely resembled that of SOM5, the regions of high pressure (Fig. 3e) experienced anomalously high maxTX values (Fig. 4a). For the WSDI, which measures persistency in extremes, anomalously high values appeared only over eastern Europe and Greenland (Fig. 4d). These spatial patterns of extremes are consistent with their trend patterns during 1979–2012, as revealed by a comparison between Figs. 1 and 4. The pattern correlation is 0.89

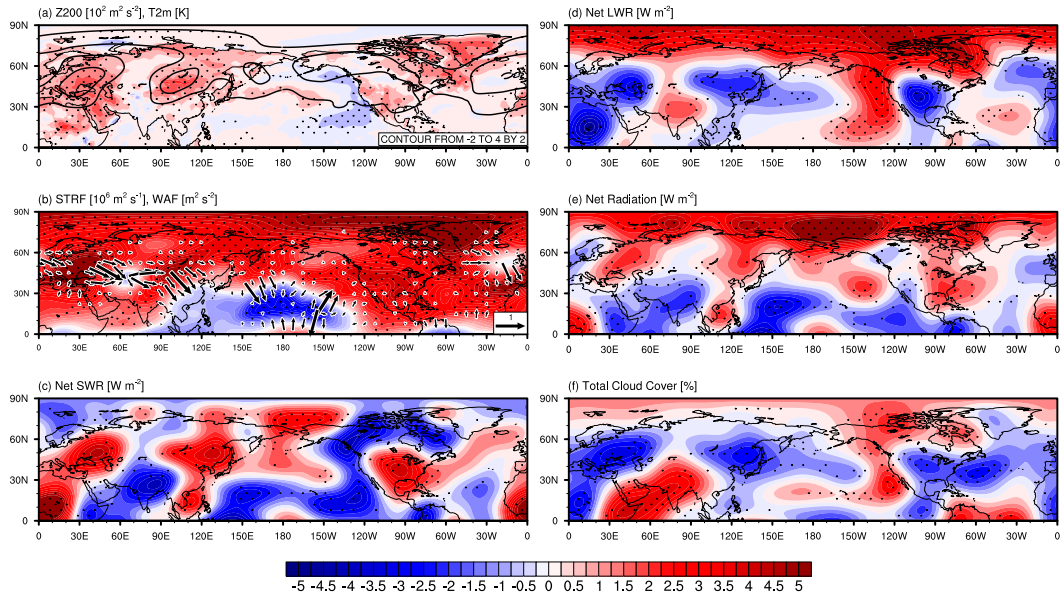


FIG. 5. Differences in (a) geopotential at 200 hPa (contours) and 2-m temperature (shading), (b) streamfunction (shading) and wave-activity flux (vectors of magnitudes larger than $0.1 \text{ m}^2 \text{ s}^{-2}$) at 200 hPa, (c) surface net solar radiation, (d) surface net infrared radiation, (e) surface net radiation, and (f) total cloud cover during P2 from those in P1. The dots denote regions in which the differences exceed the 95% confidence level as determined by the two-sided Student's *t* test.

between the trend (Fig. 1a) and the composite difference (Fig. 4a). These results indicate that the high pressure centers in SOM5 are linked to the extreme events, and suggest that the increase in occurrence of SOM5 contributed to the upward trend in the temperature extremes.

Indeed, the linkage between the intraseasonal time scale of SOM5 and the decadal time-scale shift is also evident in Fig. 5a, which shows the 1998–2012 [period 2 (P2)] minus 1979–97 [period 1 (P1)] Z200 field. This pattern of decadal change closely echoes SOM5, with a pattern correlation of 0.84. This result is consistent with the frequency time series of the SOMs (Fig. 3e) because SOM5 is the only pattern that underwent large changes after approximately 1998. Similarly, P2-minus-P1 T2m (Fig. 5a; shading), streamfunction, and wave-activity

flux (Fig. 5b) show essentially identical patterns as the corresponding SOM5-based composite fields (Figs. 6b,e). These comparisons further support the idea that part of the decadal Z200 changes are realized through changes in the frequency of intraseasonal occurrence in SOM5.

The same perspective of decadal change was presented in the context of other teleconnection patterns (Johnson and Feldstein 2010), zonal jet shifts (Lee and Feldstein 2013; Feldstein and Lee 2014), and Arctic sea ice trends (Park et al. 2015). However, this perspective does not exclude the possibility that the changes in the frequency of intraseasonal occurrence are, in the first place, caused by changes in the slowly varying background state. As was discussed by Feldstein and Lee (2014), it is possible that interdecadal forcing causes

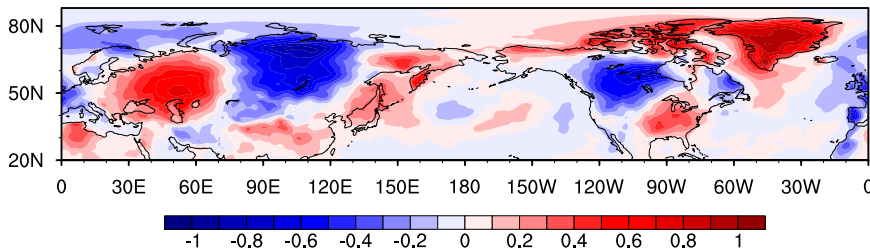


FIG. 6. Geopotential at 200 hPa ($\text{m}^2 \text{ s}^{-2}$; shading) anomaly composite of all matching days for SOM5. Prior to the composite, each year's JJA mean was subtracted. This procedure removes variability at both interannual and the long-term (1979–2012) time scales.

changes in the low-frequency background state, which then dynamically affects high-frequency subseasonal events and allows the SOM5 pattern to occur more frequently. The resulting changes in the high-frequency events may further alter the slow background flow (Wang and Lee 2016). Alternatively, it could be that the increase in the intraseasonal SOM5 occurrence is a manifestation of an additive effect caused by a long-term trend in warming. This additive effect could be a reason why the SOM5 pattern and associated temperature extremes become more frequent in the later period (1998–2012).

Radiative energy fluxes and cloud anomalies help explain how the surface temperature extremes are linked to the upper-tropospheric circulation anomalies. Figure 5c shows that downward shortwave radiation is anomalously positive within the key high pressure systems in midlatitudes. Consistently, over the same regions, cloud cover is reduced (Fig. 5f). Although the longwave cooling is also observed over the same regions, the net (downward minus upward) radiation change is still positive over the core regions (Fig. 5e). This analysis suggests the physical picture that the high pressure anomalies of the global wave train, captured by SOM5, warms the surface by allowing more shortwave radiative energy flux to be absorbed at the surface. Contributions from other thermodynamic terms, such as horizontal temperature advection, adiabatic warming, and surface heat fluxes, were found to be small (not shown). Over the Arctic, however, the effect of downward longwave radiation is greater. The dominance of infrared (IR) radiation in the Arctic thermodynamic process is consistent with the finding of Walsh and Chapman (1998). There is an emerging body of evidence that intraseasonal time-scale moisture intrusions into the Arctic play an important role for the Arctic downward IR (Doyle et al. 2011; Lee et al. 2011; Yoo et al. 2012a,b; Woods and Caballero 2016). Moreover, there is evidence that significant Arctic warming and sea ice decline during the past few decades are realized mostly through increases in moisture intrusion events (Park et al. 2015; Gong et al. 2017; Ding et al. 2017). These studies suggest that the Greenland warm core can be attributed to the midlatitude circulation south of Greenland.

The teleconnection represented by SOM5 can also help to account for interannual variability in extreme events. To investigate this possibility, we repeated the composite analysis shown in Figs. 4a and 4d except that, prior to the composite, linear trends were removed from the SOM5 frequency, maxTX, and WSDI time series. After removing the linear trend, the highest 5 years remain the same as before, but the lowest 5 years change from 1979, 1982, 1983, 1986, and 1989 for the original

data to 2009, 2004, 1997, 2003, and 1995. The detrended maxTX composite (Fig. 4b) revealed positive anomalies over part of the same key SOM5 high pressure regions such as eastern Europe, Asia, the central United States, and the west coast of Greenland. For the detrended WSDI, a positive anomaly again appeared over eastern Europe; the anomalies were insignificant in other key regions (Fig. 4e). Because SOM5 rarely occurs in the earlier period (1979–97), we also computed another version of detrended extreme indices using only the later period of 1998–2012, and then performed the same composite analysis. The results from this new calculation once again show an increase in extremes over the SOM5 centers (Figs. 4c,f), confirming our interpretation that the extreme temperatures over the SOM5 core regions are likely to be influenced by the interannual changes in the occurrence of the SOM5 pattern.

5. Subseasonal evolution of SOM5 teleconnection pattern

Given our findings that a teleconnection pattern, represented by SOM5, is closely tied to the boreal summer extreme temperatures not only in their spatial patterns but also in their interannual variability and their upward trend in frequency of occurrence, a natural question to ask is how this intraseasonal teleconnection pattern is excited. Addressing this question is beyond the scope of this study, but relevant physical process may be gleaned from the temporal evolution of the circulation and wave-activity flux (Takaya and Nakamura 2001) at 200 hPa. For this purpose, we perform a composite analysis by selecting the days for which SOM5 is the matching pattern. If two or more days occur within 15 days of each other, only the day with smallest root-mean-square errors (RMSEs) between its Z200 anomalies and SOM5 is retained for the analysis. These days are designated as lag 0 day. This selection procedure identified 57 events. To retain only intraseasonal variability, prior to the composite, we subtracted each year's JJA mean values from the data. The resulting Z200 pattern at lag 0, shown in Fig. 6, closely resembles the SOM5 pattern (Fig. 3e) that was obtained from unfiltered daily data. This consistency in the two Z200 patterns is to be expected because the time scale of SOM5 is only 4.8 days. Nevertheless, it is reassuring that the key features of the circulation pattern are intact even when only intraseasonal variability is retained in the analysis.

The composite evolution shows that there is equatorward wave-activity flux over the midlatitude western Pacific and poleward propagation over the subtropical eastern Pacific at lag -10 days (Fig. 7a). The poleward

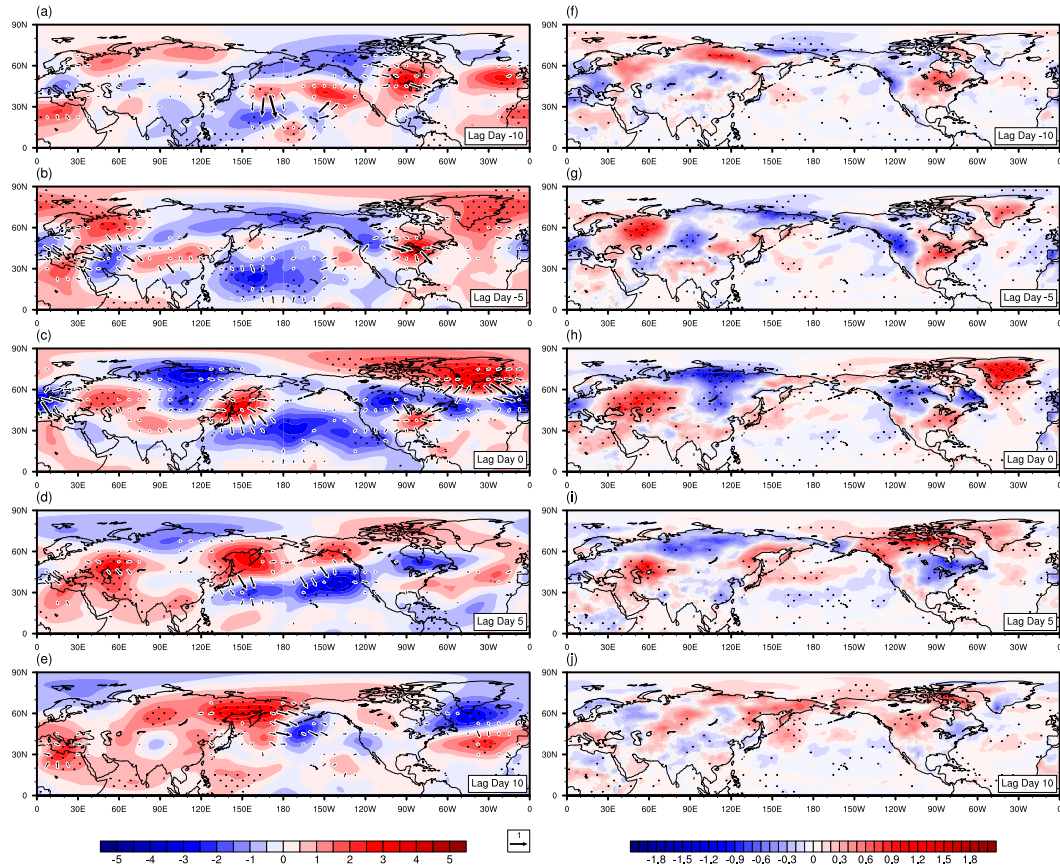


FIG. 7. Pentad evolutions of (a)–(e) streamfunction ($10^6 \text{ m}^2 \text{ s}^{-1}$; shading) and wave-activity flux ($\text{m}^2 \text{ s}^{-2}$; vector) at 200 hPa and (f)–(j) T2m (K) centering on -10 , -5 , 0 , 5 , and $+10$ days for SOM5 events. The vectors of magnitude larger than $0.1 \text{ m}^2 \text{ s}^{-2}$ are displayed. The dots denote regions in which the differences exceeded the 95% confidence level as determined by the two-sided Student's t test.

wave activity propagates toward the northeastern part of North America at lag -5 days (Fig. 7b), and then to Greenland (Fig. 7c). By lag 0 day (Fig. 7c), the poleward wave-activity flux wanes, and the anomalous high pressure system over the Canadian Arctic and Greenland is firmly established. These anomalies weaken substantially after lag $+5$ days (Figs. 7d,e).

The time sequence of poleward wave-activity flux from the tropical Pacific and the high pressure over the Arctic region suggests that forcing in the tropics may play a role for exciting the wave train over the Pacific and North America. In fact, there is a close similarity between SOM5 and the annual mean Z200 trend (1979–2012) pattern presented by Ding et al. (2014), who showed that a climate model forced by observed tropical SST trends during the same time period can produce a wave train that emanates from the Pacific to the Canadian Arctic Archipelago and Greenland. Consistent with earlier studies on the impact of tropical convection on Arctic warming (Lee et al. 2011; Yoo et al. 2012a,b;

Lee 2014), Ding et al. (2014) showed that this wave train is connected to surface warming in those Arctic regions. These findings collectively suggest that tropical forcing may contribute to the excitations of the Rossby wave train over the Pacific and North America. This possibility will be tested with a model in a follow-up study.

The accompanying 2-m temperature fields provide insight into the difference between the maxTX anomaly and WSDI anomaly. Figure 7f shows that at lag -10 days, positive anomalies were already present over eastern Europe. From lag -5 days to lag 0 day, eastern Europe continues to warm, while rapid warming occurs over Greenland (Figs. 7g,h). These warm anomalies weaken after lag $+5$ days (Figs. 7i,j). As shown in Fig. 4e, the detrended WSDI anomaly was significant only over eastern Europe, although the detrended maxTX anomaly was significant over the majority of warm regions (Fig. 4b). The time evolution examined here shows that the warm anomaly over Europe was indeed more persistent than other anomalies.

6. Concluding remarks

Motivated by observations that extreme weather events have become more frequent and that extreme weather is often associated with large-scale atmospheric circulation (Horton et al. 2015), we explored if there have been notable changes in certain large-scale features during the past few decades, and examined how such circulation patterns may be linked to extreme weather events. Based on analyses of temperature extremes and a cluster analysis of daily geopotential fields, we identify the existence of such a relationship. The circulation pattern we identify here, SOM5, is a hemispheric-scale teleconnection pattern that partially resembles a circumglobal teleconnection pattern (Branstator 2002). The extreme events tend to have complex variations in both time and space. For this reason, previous studies have focused on the extremes over small areas [e.g., DeGaetano (1996) for the United States; Heino et al. (1999) for Europe; Osborn and Jones (2000) for the United Kingdom; Zhai and Pan (2003) for China]. Our result shows that the hemisphere-wide circulation field expressed by SOM5 is linked to boreal summer extreme temperatures over several land areas.

Some useful implications follow from the fact that one of the clusters of the daily large-scale circulation fields happens to be closely tied to the major centers of temperature extremes (Europe and northeastern Asia, Arctic Canada, and Greenland). The temperature extremes over various regions are a manifestation of a Rossby wave teleconnection pattern, and the upward trend in the extremes can be understood as being a result of more frequent occurrences of the teleconnection pattern. This interpretation is supported by our findings that the teleconnection pattern grows and decays within 10 days, but that it substantially contributes to the decadal circulation trend through a dramatic increase in its intraseasonal occurrence over the decadal time scale. However, this is not to say that interdecadal forcing plays no role. It is possible that interdecadal forcing, through its influence on a slowly varying background state, also modulates the strength and frequency of the teleconnection patterns. Likewise, it is also possible that greenhouse gas-driven global warming may also modulate the strength and frequency of the pattern (Corti et al. 1999). This modulation also includes an effect of the background warming simply being added to the intraseasonal circulation pattern. Therefore, understanding how this teleconnection is excited can improve our ability to understand why temperature extremes have become more frequent.

Although examination of such a mechanism is beyond the scope of this study, our analysis supports the results

of previous studies that wave forcing from the tropical Pacific plays a role in exciting the Pacific, North America, and North Atlantic portions of the teleconnection pattern. However, it is unclear whether this tropical wave forcing can also account for the circulation and temperature anomalies over Europe and East Asia because these anomalies were present even before the onset of the tropical wave source (Figs. 7f,g). In addition, over this downstream region, the model simulation by Ding et al. (2014) does not generate SOM5-like wave train. Since remotely excited waves that reach the Arctic can also transport moisture into the region (Yoo et al. 2012a,b) and lead to cloud formation (Lee et al. 2011; Flournoy et al. 2016), it is plausible that condensational heating associated with such a transport process may play a role in exciting the downstream wave train. This possibility will be explored in the future by combining analysis of additional data and model experiments.

Acknowledgments. This research was funded by the Research Project (PE17130) and the Polar Academic Program (PE16900) of the Korea Polar Research Institute. The first author was supported by the Basic Science Research Program through the National Research Foundation of Korea (NRF) by the Ministry of Education (2012R1A1A2039645). S. Lee was supported by Seoul National University Fund.

REFERENCES

- Alexander, L. V., and Coauthors, 2006: Global observed changes in daily climate extremes of temperature and precipitation. *J. Geophys. Res.*, **111**, D05109, doi:10.1029/2005JD006290.
- Arblaster, J. M., and L. V. Alexander, 2010: The impact of the El Niño–Southern Oscillation on maximum temperature extremes. *Geophys. Res. Lett.*, **39**, L20702, doi:10.1029/2012GL053409.
- Bao, M., and J. M. Wallace, 2015: Cluster analysis of Northern Hemisphere wintertime 500-hPa flow regimes during 1920–2014. *J. Atmos. Sci.*, **72**, 3597–3608, doi:10.1175/JAS-D-15-0001.1.
- Barriopedro, D., E. M. Fischer, J. Luterbacher, R. Trigo, and R. Garcia-Herrera, 2011: The hot summer of 2010: Redrawing the temperature record map of Europe. *Science*, **332**, 220–224, doi:10.1126/science.1201224.
- Branstator, G., 2002: Circumglobal teleconnections, the jet stream waveguide, and the North Atlantic Oscillation. *J. Climate*, **15**, 1893–1910, doi:10.1175/1520-0442(2002)015<1893:CTTJSW>2.0.CO;2.
- Cai, W., and Coauthors, 2014: Increasing frequency of extreme El Niño events due to greenhouse warming. *Nat. Climate Change*, **4**, 111–116, doi:10.1038/nclimate2100.
- , and Coauthors, 2015: Increased frequency of extreme La Niña events under greenhouse warming. *Nat. Climate Change*, **5**, 132–137, doi:10.1038/nclimate2492.
- Corti, S., F. Molteni, and T. N. Palmer, 1999: Signature of recent climate change in frequencies of natural atmospheric circulation regimes. *Nature*, **398**, 799–802, doi:10.1038/19745.

- Dee, D. P., and Coauthors, 2011: The ERA-Interim reanalysis: Configuration and performance of the data assimilation system. *Quart. J. Roy. Meteor. Soc.*, **137**, 553–597, doi:10.1002/qj.828.
- DeGaetano, A. T., 1996: Recent trends in maximum and minimum temperature threshold exceedences in the northeastern United States. *J. Climate*, **9**, 1646–1660, doi:10.1175/1520-0442(1996)009<1646:RTIMAM>2.0.CO;2.
- Ding, Q., and B. Wang, 2005: Circumglobal teleconnection in the Northern Hemisphere summer. *J. Climate*, **18**, 3483–3505, doi:10.1175/JCLI3473.1.
- , J. M. Wallace, D. S. Battisti, E. J. Steig, A. J. E. Gallant, H.-J. Kim, and L. Geng, 2014: Tropical forcing of the recent rapid Arctic warming in northeastern Canada and Greenland. *Nature*, **509**, 209–212, doi:10.1038/nature13260.
- , and Coauthors, 2017: Influence of high-latitude atmospheric circulation changes on summertime Arctic sea ice. *Nat. Climate Change*, **7**, 289–295, doi:10.1038/nclimate3241.
- Dole, R., and Coauthors, 2011: Was there a basis for anticipating the 2010 Russian heat wave? *Geophys. Res. Lett.*, **38**, L06702, doi:10.1029/2010GL046582.
- Doyle, J. G., G. Lesins, C. P. Thackray, C. Perro, G. J. Nott, T. J. Duck, R. Damoah, and J. R. Drummond, 2011: Water vapor intrusions into the High Arctic during winter. *Geophys. Res. Lett.*, **38**, L12806, doi:10.1029/2011GL047493.
- Enomoto, T., B. J. Hoskins, and Y. Matsuda, 2003: The formation mechanism of the Bonin high in August. *Quart. J. Roy. Meteor. Soc.*, **129**, 157–178, doi:10.1256/qj.01.211.
- Feldstein, S. B., 2000: Teleconnections and ENSO: The timescales, power spectra, and climate noise properties. *J. Climate*, **13**, 4430–4440, doi:10.1175/1520-0442(2000)013<4430:TTPSAC>2.0.CO;2.
- , and S. Lee, 2014: Intraseasonal and interdecadal jet shifts in the Northern Hemisphere: The role of warm pool tropical convection and sea ice. *J. Climate*, **27**, 6497–6518, doi:10.1175/JCLI-D-14-00057.1.
- Flournoy, M. D., S. B. Feldstein, S. Lee, and E. E. Clothiaux, 2016: Exploring the tropically excited Arctic warming mechanism with station data: Links between tropical convection and Arctic downward infrared radiation. *J. Atmos. Sci.*, **73**, 1143–1158, doi:10.1175/JAS-D-14-0271.1.
- Gong, T., S. B. Feldstein, and S. Lee, 2017: The role of downward infrared radiation in the recent Arctic winter warming trend. *J. Climate*, **30**, 4937–4949, doi:10.1175/JCLI-D-16-0180.1.
- Goss, M., S. B. Feldstein, and S. Lee, 2016: Stationary wave interference and its relation to tropical convection and Arctic warming. *J. Climate*, **29**, 1369–1389, doi:10.1175/JCLI-D-15-0267.1.
- Ha, K.-J., J.-E. Chu, J.-Y. Lee, B. Wang, S. N. Hameed, and M. Watanabe, 2012: What caused the cool summer over northern central Asia, East Asia and central North America during 2009? *Environ. Res. Lett.*, **7**, 044015, doi:10.1088/1748-9326/7/4/044015.
- Hansen, J., R. Ruedy, M. Sato, and K. Lo, 2010: Global surface temperature change. *Rev. Geophys.*, **48**, RG4004, doi:10.1029/2010RG000345.
- Heino, R., and Coauthors, 1999: Progress in the study of climatic extremes in northern and central Europe. *Climatic Change*, **42**, 151–181, doi:10.1023/A:1005420400462.
- Hong, C.-C., H.-H. Hsu, N.-H. Lin, and H. Chiu, 2011: Role of European blocking and tropical–extratropical interaction in the 2010 Pakistan flooding. *Geophys. Res. Lett.*, **38**, L13806, doi:10.1029/2011GL047583.
- Horton, D. E., N. C. Johnson, D. Singh, D. L. Swain, B. Rajaratnam, and N. S. Diffenbaugh, 2015: Contribution of changes in atmospheric circulation patterns to extreme temperature trends. *Nature*, **522**, 465–469, doi:10.1038/nature14550.
- Huber, D. G., and J. Gullede, 2011: Extreme weather and climate change: Understanding the link and managing the risk. Science and Impacts Program, Center for Climate and Energy Solutions. [Available online at <http://www.c2es.org/publications/extreme-weather-and-climate-change>.]
- IPCC, 2012: Summary for policymakers. *Managing the Risks of Extreme Events and Disasters to Advance Climate Change Adaptation*, C. B. Field et al., Eds., Cambridge University Press, 1–19.
- Johnson, N. C., 2013: How many ENSO flavors can we distinguish? *J. Climate*, **26**, 4816–4827, doi:10.1175/JCLI-D-12-00649.1.
- , and S. B. Feldstein, 2010: The continuum of North Pacific sea level pressure patterns: Intraseasonal, interannual, and interdecadal variability. *J. Climate*, **23**, 851–867, doi:10.1175/2009JCLI3099.1.
- , —, and B. Tremblay, 2008: The continuum of Northern Hemisphere teleconnection patterns and a description of the NAO shift with the use of self-organizing maps. *J. Climate*, **21**, 6354–6371, doi:10.1175/2008JCLI2380.1.
- Kohonen, T., 2001: *Self-Organizing Maps*. 3rd ed. Springer, 521 pp.
- Lau, N.-C., 1997: Interaction between global SST anomalies and the midlatitude atmospheric circulation. *Bull. Amer. Meteor. Soc.*, **78**, 21–33, doi:10.1175/1520-0477(1997)078<0021:IBGSA>2.0.CO;2.
- Lau, W. K. M., and K.-M. Kim, 2012: The 2010 Pakistan flood and Russian heat wave: Teleconnection of hydrometeorology extremes. *J. Hydrometeorol.*, **13**, 392–403, doi:10.1175/JHM-D-11-016.1.
- Lee, M.-H., C.-H. Ho, J. Kim, and C.-K. Song, 2012: Assessment of the changes in extreme vulnerability over East Asia due to global warming. *Climatic Change*, **113**, 301–321, doi:10.1007/s10584-011-0345-9.
- Lee, S., 2014: A theory for polar amplification from a general circulation perspective. *Asia-Pac. J. Atmospheric Sci.*, **50**, 31–43, doi:10.1007/s13143-014-0024-7.
- , and S. B. Feldstein, 2013: Detecting ozone- and greenhouse gas–driven wind trends with observational data. *Science*, **339**, 563–567, doi:10.1126/science.1225154.
- , T. Gong, N. Johnson, S. B. Feldstein, and D. Pollard, 2011: On the possible link between tropical convection and the Northern Hemisphere Arctic surface air temperature change between 1958 and 2001. *J. Climate*, **24**, 4350–4367, doi:10.1175/2011JCLI4003.1.
- Leith, C. E., 1973: The standard error of time-averaged estimates of climatic means. *J. Appl. Meteor.*, **12**, 1066–1069, doi:10.1175/1520-0450(1973)012<1066:TSEOTA>2.0.CO;2.
- Leloup, J., Z. Lachkar, J.-P. Boulanger, and S. Thiria, 2007: Detecting decadal changes in ENSO using neural networks. *Climatic Dyn.*, **28**, 147–162, doi:10.1007/s00382-006-0173-1.
- Liu, Y., R. H. Weisberg, and C. N. K. Mooers, 2006: Performance evaluation of the self-organizing map for feature extraction. *J. Geophys. Res.*, **111**, C05018, doi:10.1029/2005JC003117.
- Madden, R. A., 1976: Estimates of the natural variability of time averaged sea-level pressure. *Mon. Wea. Rev.*, **104**, 942–952, doi:10.1175/1520-0493(1976)104<0942:EOTNVO>2.0.CO;2.
- Osborn, T. J., and P. D. Jones, 2000: Air flow influences on local climate: Observed United Kingdom climate variations. *Atmos. Sci. Lett.*, **1**, 62–74, doi:10.1006/asle.2000.0013.

- Park, D.-S. R., S. Lee, and S. B. Feldstein, 2015: Attribution of the recent winter sea ice decline over the Atlantic sector of the Arctic Ocean. *J. Climate*, **28**, 4027–4033, doi:[10.1175/JCLI-D-15-0042.1](https://doi.org/10.1175/JCLI-D-15-0042.1).
- Peterson, T. C., and M. J. Manton, 2008: Monitoring changes in climate extremes: A tale of international collaboration. *Bull. Amer. Meteor. Soc.*, **89**, 1266–1271, doi:[10.1175/2008BAMS2501.1](https://doi.org/10.1175/2008BAMS2501.1).
- Rahmstorf, S., and D. Coumou, 2011: Increase of extreme events in a warming world. *Proc. Natl. Acad. Sci. USA*, **108**, 17 905–17 909, doi:[10.1073/pnas.1101766108](https://doi.org/10.1073/pnas.1101766108).
- Saeed, S., N. Van Lipzig, W. A. Müller, F. Saeed, and D. Zanchettin, 2014: Influence of the circumglobal wave-train on European summer precipitation. *Climate Dyn.*, **43**, 503–515, doi:[10.1007/s00382-013-1871-0](https://doi.org/10.1007/s00382-013-1871-0).
- Schneidererit, A., S. Schubert, P. Vargin, F. Lunkeit, X. Zhu, D. H. W. Peters, and K. Fraedrich, 2012: Large-scale flow and the long-lasting blocking high over Russia: Summer 2010. *Mon. Wea. Rev.*, **140**, 2967–2981, doi:[10.1175/MWR-D-11-00249.1](https://doi.org/10.1175/MWR-D-11-00249.1).
- Seneviratne, S. I., M. G. Donat, B. Mueller, and L. V. Alexander, 2014: No pause in the increase of hot temperature extremes. *Nat. Climate Change*, **4**, 161–163, doi:[10.1038/nclimate2145](https://doi.org/10.1038/nclimate2145).
- Takaya, K., and H. Nakamura, 2001: A formation of a phase-independent wave-activity flux for stationary and migratory quasi-geostrophic eddies on a zonally varying basic flow. *J. Atmos. Sci.*, **58**, 608–627, doi:[10.1175/1520-0469\(2001\)058<0608:AFOAPI>2.0.CO;2](https://doi.org/10.1175/1520-0469(2001)058<0608:AFOAPI>2.0.CO;2).
- Teng, H., G. Branstator, H. Wang, G. A. Meehl, and W. M. Washington, 2013: Probability of US heat waves affected by a subseasonal planetary wave pattern. *Nat. Geosci.*, **6**, 1056–1061, doi:[10.1038/ngeo1988](https://doi.org/10.1038/ngeo1988).
- Trenberth, K. E., and Coauthors, 2007: Observations: Surface and atmospheric climate change. *Climate Change 2007: The Physical Science Basis*, S. Solomon et al., Eds., Cambridge University Press, 235–336.
- Walsh, J. E., and W. L. Chapman, 1998: Arctic cloud–radiation–temperature associations in observational data and atmospheric reanalyses. *J. Climate*, **11**, 3030–3045, doi:[10.1175/1520-0442\(1998\)011<3030:ACRTAI>2.0.CO;2](https://doi.org/10.1175/1520-0442(1998)011<3030:ACRTAI>2.0.CO;2).
- Wang, H., B. Wang, F. Huang, Q. Ding, and J.-Y. Lee, 2012: Interdecadal change of the boreal summer circumglobal teleconnection (1958–2010). *Geophys. Res. Lett.*, **39**, L12704, doi:[10.1029/2012GL052371](https://doi.org/10.1029/2012GL052371).
- Wang, L., and S. Lee, 2016: The role of eddy diffusivity on poleward jet shift. *J. Atmos. Sci.*, **73**, 4945–4958, doi:[10.1175/JAS-D-16-0082.1](https://doi.org/10.1175/JAS-D-16-0082.1).
- Ward, J. H., Jr., 1963: Hierarchical grouping to optimize an objective function. *J. Amer. Stat. Assoc.*, **58**, 236–244, doi:[10.1080/01621459.1963.10500845](https://doi.org/10.1080/01621459.1963.10500845).
- Woods, C., and R. Caballero, 2016: The role of moist intrusions in winter Arctic warming and sea ice decline. *J. Climate*, **29**, 4473–4485, doi:[10.1175/JCLI-D-15-0773.1](https://doi.org/10.1175/JCLI-D-15-0773.1).
- Xu, G., Y. Zong, and Z. Yang, 2013: *Applied Data Mining*. CRC Press, 284 pp.
- Yoo, C., S. Lee, and S. B. Feldstein, 2012a: Arctic response to an MJO-like tropical heating in an idealized GCM. *J. Atmos. Sci.*, **69**, 2379–2393, doi:[10.1175/JAS-D-11-0261.1](https://doi.org/10.1175/JAS-D-11-0261.1).
- , —, and —, 2012b: Mechanisms of Arctic surface air temperature change in response to the Madden–Julian oscillation. *J. Climate*, **25**, 5777–5790, doi:[10.1175/JCLI-D-11-00566.1](https://doi.org/10.1175/JCLI-D-11-00566.1).
- Yuan, J., B. Tan, S. B. Feldstein, and S. Lee, 2015: Wintertime North Pacific teleconnection patterns: Seasonal and interannual variability. *J. Climate*, **28**, 8247–8263, doi:[10.1175/JCLI-D-14-00749.1](https://doi.org/10.1175/JCLI-D-14-00749.1).
- Zhai, P. M., and X. H. Pan, 2003: Trends in temperature extremes during 1951–1999 in China. *Geophys. Res. Lett.*, **30**, 1913, doi:[10.1029/2003GL018004](https://doi.org/10.1029/2003GL018004).